

Chapter 2

Neural crest–placode interactions mediate trigeminal ganglion formation and require Slit1–Robo2 signaling

2.1 Abstract¹

The cellular and molecular interactions allowing generation of complex cranial sensory ganglia remain unknown. Here, we show that proper formation of the trigeminal ganglion, the largest of the cranial ganglia, relies on intimate and bi-directional interactions between its two precursor cell types, placodal and neural crest cells. Removal of either population results in severe defects. We show that placodal and neural crest cells concurrently express the receptor–ligand pair, Robo2 and Slit1, respectively, during a discrete time window consistent with their potential role in initial placode–neural crest interactions and early ganglion assembly. Perturbation of this receptor–ligand interaction by blocking Robo2 function or depleting either Robo2 or Slit1 using RNA interference (RNAi) disrupts proper placodal ganglion formation which mimics the effects of ablating the neural crest. Inhibition of Robo2 in placodal cells also causes wild-type neural crest cells to aberrantly assemble with the affected placodal neurons into severely disorganized ganglia. This non-cell-autonomous effect further underscores the reciprocal neural crest–placode relationship. Our data suggest that signaling from the neural crest through Slit1–Robo2 acts as a positive regulator of placodal ingression, cell positioning, and/or axon guidance during trigeminal gangliogenesis. Thus, our data reveal for the first time, a

¹ This chapter is based on Shiau CE, Lwigale, PY, Das RM, Wilson SA, Bronner-Fraser M. Robo2–Slit1 dependent cell-cell interactions mediate assembly of the trigeminal ganglion. *Nat. Neurosci.* 2008 Mar; 11(3): 269-76.

putative molecular signaling event underlying neural crest–placode interactions during gangliogenesis, representing a novel and essential role for Slit–Robo in cell–cell interactions during vertebrate development.

2.2 Introduction

The origin of sensory ganglia in the developing peripheral nervous system can be traced to two transient embryonic cell populations: the neural crest and ectodermal placodes (D'Amico-Martel and Noden, 1983). Both cell types contribute to specialized structures that distinguish vertebrates from other chordates. Neural crest cells form at the dorsal-most portion of the neural tube, undergo extensive migrations and differentiate into a plethora of derivatives, including sensory and autonomic ganglia, cranial cartilage and bone, and pigment cells (Knecht and Bronner-Fraser, 2002). Placodes are transient regions of thickened head ectoderm that form on the surface epithelium lateral to the cranial neural tube. They ingress into the mesenchyme to form cranial sensory ganglia as well as essential components of the paired sense organs, contributing to lens, nose, and ears (Baker and Bronner-Fraser, 2001).

A fundamental question in gangliogenesis is how precursors interact and organize themselves to later form an anatomically correct structure with proper connections to the central nervous system and its sensory organs. The trigeminal ganglion, responsible for the senses of touch, pain, and temperature of much of the face and jaws, is the largest of the cranial ganglia and a prime example of one with dual neural crest and placode origin. Tissue ablation experiments suggest that neural crest–placode cell interactions are critical

for formation of the trigeminal ganglion (Hamburger, 1961; Lwigale, 2001), though the underlying molecular mechanism remains unknown.

The formation of ganglia from neural crest and/or placode populations involves several discrete steps. First, precursor cells delaminate by undergoing an epithelial-to-mesenchymal transition. Second, the cells migrate as individuals to the site of ganglion formation. Third, they aggregate and condense to form discrete ganglia of the sensory nervous system. For neural crest, several cell surface receptors and cell adhesion molecules have been implicated as molecular mediators of this three-step process. The epithelial-to-mesenchymal transition that results in their delamination from the neural tube involves loss of Cadherin-6b which is directly down-regulated by the transcriptional repressor and neural crest marker, Snail2 (Taneyhill et al., 2007). Several types of cell-cell and cell-matrix interactions have been implicated in guiding cranial and/or trunk neural crest migration to sites of peripheral ganglion formation, including Eph-ephrin (Kasemeier-Kulesa et al., 2006; Krull et al., 1997), neuropilin-Semaphorin (Gammill et al., 2006), laminin- (Coles et al., 2006) and integrin- (Kil et al., 1998) extracellular matrix interactions. Finally, N-cadherin has been suggested to mediate their condensation into discrete dorsal root and sympathetic ganglia (Akitaya and Bronner-Fraser, 1992; Kasemeier-Kulesa et al., 2006). In contrast to neural crest, virtually nothing is known about the molecular events involved in formation of placode-derived ganglia.

In the present study, we test the role of Robo-Slit interactions in formation of the trigeminal ganglion. Slits and their Robo receptors (Brose et al., 1999; Kidd et al., 1999) are evolutionarily conserved regulators present in the developing nervous system of diverse animals ranging from nematodes and fruit flies to vertebrates (Chedotal, 2007). Although best known for mediating repulsion, they also can promote axon branching (Zinn and Sun, 1999) and cell migration (Kramer et al., 2001) and, in *Drosophila*, have been implicated for novel roles in cell adhesion and morphogenesis of the forming heart tube (Santiago-

Martinez et al., 2006). In vertebrates, they have broad expression patterns in diverse tissues including teeth (Loes et al., 2001), lungs (Anselmo et al., 2003), limbs (Vargesson et al., 2001), and kidneys (Piper et al., 2000). Here, we show that neural crest and placode cells express Slit and Robo respectively, in a complementary manner and that the organization of the trigeminal ganglion is lost when either receptor or ligand is inhibited. Our results provide novel insights into the mechanisms underlying cranial gangliogenesis. They suggest a major role for the receptor, Robo2, in mediating this process, representing one of the first examples of Robo–Slit signaling in cell–cell interactions in vertebrate development.

2.3 Materials and methods

Embryos

Fertilized chicken (*Gallus gallus domesticus*) and quail (*Coturnix coturnix japonica*) eggs were obtained from local commercial sources and incubated at 37°C to the desired stages according to the Hamburger and Hamilton staging system.

In situ hybridization

Whole mount chick in situ hybridization was performed as previously described (Kee and Bronner-Fraser, 2001). cDNA templates used for antisense riboprobes were: chick Slits 1–3 and Robos 1–2 as described (Vargesson et al., 2001), and Sox10 (Cheng et al., 2000). Embryos were imaged and subsequently sectioned at 12–14 µm.

Immunohistochemistry

Primary antibodies used were anti-GFP (Molecular Probes), anti-HNK-1 (American Type Culture), anti-QCPN (quail specific nuclear marker) (DSHB), anti-Islet1 (DSHB), and anti-TuJ1 (Covance), as described in Appendix B. Staining was performed on whole embryos or 12 μm sections. Images were taken using the AxioVision software from a Zeiss Axioskop2 plus fluorescence microscope, and processed using Adobe Photoshop CS3.

In ovo electroporation of the trigeminal ectoderm or presumptive neural crest

Chick embryos (stages 8–10 for placode electroporation and stages 4–9 for neural crest electroporation) were injected with the DNA or miRNA vector of interest. Platinum electrodes were placed vertically or horizontally across the embryo using various electroporation conditions, as further described in Appendix B. Plasmid DNA vectors driven by a chick β -actin promoter with a CMV enhancer were used as follows: Robo2 Δ -GFP (Hammond et al., 2005), and for control GFP expression, cytoplasmic pCIG (cyto-pCIG)(see Appendix B) and pCA β -IRES-mGFP (McLarren et al., 2003).

Ecto-mesenchyme culture

Either the neural crest or the placode tissue was electroporated with cyto-pCIG as described above. The surface ectoderm and the adherent underlying mesenchyme in the presumptive trigeminal region demarcated in Fig. 3g was explanted and cultured in either 4- or 8- well chamber mounted on glass slides (Lab-TekII, NUNC) treated with 25 $\mu\text{g}/\text{ml}$ fibronectin in F12/N2 serum free medium in a 7% CO₂ incubator at 37°C for ~20 hours.

Neural fold and ectoderm tissue ablations

Ablations were performed as previously described (Lwigale, 2001) with slight modifications, as described in Appendix B.

GFP labeling of the ectoderm combined with quail-chick grafts

Ectoderm electroporation with cyto-pCIG was performed on stage 9 (6–7 somites) chick embryos followed by a quail-chick neural fold graft, as described in Appendix B.

Quail-chick grafts combined with ectoderm tissue ablation

Quail-chick grafting of the neural folds in stage 9 (6–7ss) chick embryos was performed as described above. Chimeras were then re-opened at about stage 12 and the presumptive trigeminal ectoderm was ablated as aforementioned.

Analysis of Islet1+ placode cells during ingression

Percentages of Islet1+ cells associated with the ectoderm (in the ectoderm and associated with its basal margin) and in the mesenchyme were calculated from dividing the number of Islet1+ cells in the respective regions by the total number of Islet1+ cells in the entire presumptive trigeminal area (Fig. 7i, dotted box); cells were counted from frontal plane sections (12 μ m). Details are described in Appendix B. Statistical significance was determined by a two-tailed student's t-test assuming equal variances.

RNAi

Electroporations were performed as described above. RNAi vectors were constructed as described previously (Das et al., 2006) with slight modification as described in Appendix B. Target sequences used were 5' GGCACAAGCTGGAGTACAATA (GFP) (Das et al., 2006), 5' GCTCTAATCTGTATGGATCTAA (Robo2), and 5' CTGCCAGTGCCGAG

ACCATCAA (Slit1). Rescue was performed with a full length mouse Slit1-myc fusion construct (Yuan et al., 1999).

2.4 Results

2.4.1 Cell–cell interactions during ganglion assembly

In the chick embryo, trigeminal placode cells begin to ingress at ~stage 12 (D'Amico-Martel and Noden, 1983), intermixing with a stream of migratory cranial crest cells. To better understand the behavior of neural crest and placode cells during trigeminal ganglion formation, we first carefully established the timing of their interactions at successive stages (Figs. 1 and 2) and examined their cell–cell associations using tissue-specific grafts or electroporation of GFP coupled with molecular markers (Figs. 1 and 3).

Ingression of trigeminal placode cells from the surface ectoderm peaks between stages 14–16 and ceases at ~stage 21 (D'Amico-Martel and Noden, 1983). Prior to ingression, placode cells co-express neuronal markers, *Islet1* (Begbie et al., 2002) and β -neurotubulin (TuJ1) (Moody et al., 1989), as early as stages 12–13 and continue to express these markers throughout gangliogenesis (Figs. 1, 2, 3a–c). By the time placode and neural crest cells come into close contact, placode cells express neuronal markers, but are not necessarily post-mitotic as these markers also label dividing neuroblasts (Begbie et al., 2002; Moody et al., 1989). Post-mitotic placode-derived neurons are first observed at stage 16 (D'Amico-Martel and Noden, 1980). Neural crest cells, on the other hand, only begin neuronal differentiation at embryonic day 4 (D'Amico-Martel and Noden, 1980), which is equivalent to stages ~22–24. *Islet1* and TuJ1 were specific for placode cells prior to this

stage, as shown by colocalization of these markers with GFP introduced in presumptive placode cells; in contrast, their expression failed to overlap with GFP-labeled neural crest cells at stages 16–18 (Fig. 2 and data not shown).

By stage 13, placode cells enter the subectodermal region and mingle with already present neural crest cells that express HNK-1 antigen (Fig. 3a,b). Placode cells ingress as individuals or in short chains and appear to maintain contact with each other in the cranial mesenchyme (Fig. 3b). At stage 13, placode-derived neuroblasts have short, randomly oriented axons (Fig. 3a,b); in the condensing ganglion at stage 17, most axons have aligned along the proximodistal axis (Fig. 3c).

To perform a detailed analysis of associations between placode and neural crest cells in the forming ganglion, we used quail/chick dorsal neural tube grafts coupled with GFP electroporation of the ectoderm in the same embryos (Fig. 3d–f). The trigeminal ganglia of these embryos are well condensed into a stereotypic bi-lobed structure comprised of ophthalmic (OpV) and maxillo-mandibular (MmV) branches. By stage 18, quail-derived trigeminal neural crest cells are intermixed with GFP-expressing placode neurons and have segregated from the rest of the midbrain crest stream that now surrounds the eye and occupies the first branchial arch (Fig. 3e). Neural crest and placode cells are observed throughout the ganglion, with the exception of the most proximal portion, which is solely neural crest-derived (Fig. 3f). This prefigures the segregation of neural crest-derived neurons in the proximal portion and placode-derived neurons in the distal part of the ganglion in the nearly mature ganglion at embryonic day 12 (stage 38) (D'Amico-Martel and Noden, 1983). These results show that throughout gangliogenesis, the trigeminal precursor cells intermingle and are in direct contact with each other. To further examine placode–neural crest interactions, we developed an ecto-mesenchyme culture system (Fig. 3g). We labeled the two cell types by *in ovo* electroporation with a GFP expression construct introduced into either the presumptive neural tube or ectoderm.

Trigeminal tissue was then explanted, encompassing both the placodal ectoderm and adherent underlying mesenchyme from stage 13 embryos, coinciding with the time of predicted cell–cell interactions. By visualizing the degree of contact, we found that the two cell populations remained tightly associated and intermingled. They exhibited abundant processes and regions of close cell–cell association (Fig. 3h–k). This raised the intriguing possibility that cell–cell interactions between placode and neural crest cells may mediate gangliogenesis.

2.4.2 Expression of Robo2 on placodes and Slit1 on neural crest

We next investigated whether Robo receptors and their cognate Slit ligands were good candidates for mediators of trigeminal ganglion formation by examining their gene expression patterns. Robos 1–2 receptors can bind to all three Slits with comparable affinity (Brose et al., 1999). We found that Robo2, but not Robo1, transcript is present in the trigeminal ganglion and its precursors during gangliogenesis. By stage 12, Robo2 is expressed in the ectoderm adjacent to the presumptive midbrain (Fig. 4a), in the region fated to give rise to the trigeminal placodes (D'Amico-Martel and Noden, 1983). Conversely, Slit1, but not Slit2 or Slit3, transcript is expressed by migratory midbrain and anterior hindbrain neural crest cells that contribute to the trigeminal ganglion (Fig. 4b). Trigeminal placode cells continue to express Robo2 as they ingress and intermix with migratory neural crest cells at stage 14 (Fig. 4c) and through trigeminal ganglion formation at stage 18, with the MmV lobe having an apparently weaker Robo2 signal than the OpV (Fig. 4d). In contrast, Slit1 is transiently expressed during cranial neural crest migration (Fig. 4e) and down-regulated in the ganglion by stage 18 (Fig. 4f).

Robo2 expressing GFP-labeled placode cells intermix with migratory neural crest cells (Fig. 4g,h) at times when neural crest cells are expressing Slit1 (Fig. 4i,j) during

stages 13–14. Robo2 appears to be expressed in discrete, dispersed regions in the surface ectoderm (Fig. 4g,h), characteristic of cells about to detach. All ingressed GFP positive cells are also Robo2 positive. Thus, Robo2 appears to begin marking placode cells that are either ingressing or preparing to do so. Our results show that placode and neural crest cells concurrently express the receptor–ligand pair, Robo2 and Slit1, respectively, during a discrete time window consistent with their potential role in initial placode–neural crest interactions and early ganglion assembly.

2.4.3 Placode and neural crest cells interact reciprocally

If placode–neural crest interactions are indeed important for trigeminal ganglion formation, removal of either population should result in abnormal development, including possible reduction or malformation of the ganglion. To determine the importance of heterotypic cell interactions, we first ablated the placode population and assessed its effect on the neural crest. Ablation of presumptive placodal ectoderm resulted in loss of the placodal markers, β -neurotubulin (TuJ1) and Robo2 (Fig. 5a), verifying removal of most of the tissue. After placode removal, the neural crest population did not coalesce properly into the ganglion (Fig. 5a,b). Instead, the cells appeared dispersed or shifted toward the periocular region. In fact, condensed neural crest cells were only observed in regions where some residual placode cells were present (Fig. 5b).

For the reciprocal experiment, neural folds (containing presumptive neural crest cells) were ablated and the subsequent effects on placode development examined. This resulted in the loss of most, but not all, of the neural crest marker, Sox10 (Cheng et al., 2000) (Fig. 5a). Removal of the majority of neural crest cells led to failure of trigeminal placode cells to make proper connections to the hindbrain, similar to the case previously observed for epibranchial ganglia (Begbie and Graham, 2001a). In addition, these cells

failed to integrate into a single trigeminal ganglion (Fig. 5a). This effect was most striking in the OpV region where placode cells often condense in one large and several smaller clusters of cells and exhibit disorganized axonal projections. In contrast, neural crest ablation does not appear to affect placodal ingression or differentiation since placodal cells continue to express neuronal markers (TuJ1 and Islet1) and Robo2. Taken together, these results suggest essential but distinct roles of neural crest and placodes for proper ganglion formation. Neural crest cells appear to make a scaffold that integrates placode cells into a properly shaped ganglion with appropriate connections to the hindbrain, though the latter defect may be partially due to incomplete neural tube closure following ablation. Placode cells, on the other hand, act as crucial mediators of neural crest condensation. This raises the intriguing possibility that intercellular signaling between these two cell types may coordinate gangliogenesis.

2.4.4 Robo2 function is required for proper gangliogenesis

To test a potential role for Robo signaling during ganglion formation, we sought to block the function of Robo2 *in vivo*. To this end, we introduced by electroporation into the trigeminal ectoderm a GFP-tagged dominant-negative version of the Robo2 receptor (Robo2 Δ -GFP) (Hammond et al., 2005) that lacks the intracellular domains required for signaling. Embryos electroporated at stages 8–10 were examined either at early stages of ganglion formation (stages 15–16) or after the ganglion had condensed (stages 17–18).

The results show that in contrast to control GFP electroporated embryos (Fig. 6a–c), perturbation of Robo2 signaling inhibits proper assembly of placode cells, causing the ganglion to assume a highly dispersed morphology (78.6% in OpV and 16.7% in MmV) (Fig. 6d–f) at stages 15–16. This was shown by both displacement of placode neuronal cell bodies and misorientation of axonal projections (Fig. 6e,f). By stages 17–18,

placode-derived neurons have coalesced normally in control embryos (Fig. 6g–i) but abnormally in multiple or branch-like aggregates (57.1% in OpV; 7.7% in MmV) in Robo2 Δ -GFP electroporated embryos (Fig. 6j–l). Both the OpV and MmV nerve fibers failed to properly fasciculate towards their normal targets. The effects were highly reminiscent of those following neural crest ablation, with more severe defects in the OpV than the MmV lobes. For both experimental and control cases, we scored only those embryos with broad GFP expression in most of either the OpV, MmV or both lobes. Statistical analyses of these embryos are summarized in Fig. 6m,n.

2.4.5 Perturbation of Robo2 disrupts placode ingression.

To examine whether Robo2 plays an important function in placodal ingression, we next examined the effects of blocking its signaling at stage 14, reflecting the time of maximal interactions between ingressing placode cells and migratory neural crest cells that express Slit1. Compared with stage-matched controls (Fig. 7a–c), in Robo2 Δ -GFP embryos trigeminal placode cells appeared more dispersed (Fig. 7d–f). In contrast to controls where most placode cells have ingressed into the neural crest derived mesenchyme (Fig. 7g), the majority either remained in the surface ectoderm or associated with the basal margin of the ectoderm (Fig. 7h), suggesting a defect in placodal ingression and/or migration. The percentage of placode cells associated with the ectoderm in the Robo2 Δ -GFP embryos (64.2 ± 8.6 %) was significantly higher than those in the control embryos (25.6 ± 4.2 %; $P < 0.0001$, two-tailed t-test assuming equal variances) (Fig. 7i).

This is likely to reflect a delay rather than inhibition of cell movement since most Robo2 Δ -GFP expressing placode cells migrated into the mesenchyme by stages 17–18 (data not shown). Thus, blocking Robo2 signaling appears to cause placode cells to remain

in the surface ectoderm for an abnormally long time, thereby delaying their interactions with neural crest cells until times when the latter has down-regulated the Slit1 ligand.

2.4.6 Effect of Robo2 perturbation on neural crest assembly

In contrast to its effects on placode ingression, inhibition of the Robo2 signaling in the ectoderm does not alter neural crest migration (Fig. 8e). However, unlike control embryos (Fig. 8a), during later stages as the ganglion assembles, neural crest cells, as assayed by Sox10 expression, are abnormally localized in a pattern that mirrors the abnormal organization of the placode cells with blocked Robo2 signaling (Fig. 8b,c).

Intriguingly, this phenocopies the effects of placode ablation where the neural crest cells appear to aggregate in the same places as the residual placode cells. Transverse sections through the OpV region of these embryos reveal clustering of Sox10 expressing neural crest cells with Robo2 Δ -GFP expressing placode cells (Fig. 8b,c). Since Robo2 Δ -GFP encodes a membrane-tethered construct, the effects are non-cell autonomous and likely mediated by interactions between aberrantly disorganized placode cells expressing Robo2 Δ -GFP and the affected wild type neural crest cells.

2.4.7 RNAi knockdowns of Robo2 and Slit1 cause ganglion defects.

Use of a dominant negative construct has the caveat that it is likely to perturb all Robos rather than being specific for Robo2; in addition, it interferes with all Slits. To specifically test the role of Robo2 and Slit1 in trigeminal ganglion formation, we turned to an alternative approach using RNA interference (RNAi) mediated knockdown. To this end, we used synthetic microRNA (miRNA) vectors designed to selectively target Robo2 or Slit1, while concomitantly expressing RFP (Das et al., 2006).

Electroporation of Robo2 miRNA into the placodal ectoderm at stages 8–10, prior to ingression, caused reduction of Robo2 mRNA levels in the forming ganglia (Fig. 9) but had no effect on the placodal marker, Pax3 (data not shown). Analyzing ganglion formation by similar criteria to those employed for Robo2 Δ -GFP above, Robo2 RNAi affected placode cells in a manner that phenotypically resembled that of the dominant negative construct with more severe defects in the OpV than the MmV lobe (Fig. 10). Compared to controls (Fig. 10a–c), trigeminal placode neurons transfected with Robo2 miRNA tended to form dispersed aggregates and elaborated abnormal and branched projections (Fig. 10d–f). These effects were similar but generally less severe than those noted with the dominant negative construct, likely because of incomplete knockdown since message levels were decreased but not eliminated by the miRNA. To control for non-specific effects of the backbone RNAi vector, we performed parallel experiments using the GFP miRNA which targets GFP. Although the control RNAi caused some general toxicity when introduced into the ectoderm, effects of the Robo2 miRNA were markedly more severe, specific, and distinguishable.

To examine the functional role of the Slit1 ligand, we introduced the Slit1 miRNA in the presumptive neural crest tissue by electroporation at stages 4–9. Slit1 miRNA resulted in a depletion but not absence of Slit1 on the electroporated side (Fig. 9). At stages of ganglion formation, compared to the control GFP miRNA electroporated embryos (Fig. 10g–i), Slit1 miRNA mediated depletion of Slit1 in the neural crest caused aberrant assembly of placode cells such that they aggregated abnormally in dispersed clumps and tended to form OpV and MmV lobes that were either misaligned or appeared closely apposed in the interlobic region (Fig. 10j–l). To control for possible off-target effects, we examined other neural crest markers after Slit1 miRNA as well as performed rescue experiments with a mouse Slit1 construct. Slit1 miRNA had no effect on neural crest markers, such as Slug and HNK-1; furthermore, co-electroporation with mouse Slit1

resulted in a significant rescue of the numbers of abnormal ganglia, from ~50% to 20% (n = 10, data not shown). Statistical analyses of Robo2 miRNA and Slit1 miRNA embryos are summarized in Fig. 10m,n.

Taken together, abrogating Robo2–Slit1 interaction with dominant negative Robo2, Robo2 miRNA or Slit1 miRNA mimics the effects of neural crest ablation. This suggests a mechanism whereby signaling between this receptor/ligand pair underlies interactions between neural crest and placodal cells in trigeminal ganglion formation.

2.5 Discussions

2.5.1 Tissue ablations uncover reciprocal neural crest–placode interactions

Tissue ablation experiments suggest that interactions between placode and neural crest cells are critical for formation of the trigeminal ganglion. However, the cellular and molecular nature of these interactions has been an open question. Here, we apply a combination of classical embryological and modern molecular techniques to solve this long-standing puzzle. Our data show that proper assembly of the trigeminal ganglion relies on the intimate and coordinated interactions of placode and neural crest cells, such that removal of either cell populations results in striking defects in ganglion formation. Our results are consistent with previous ablation studies, noting dispersed (Hamburger, 1961) or smaller ganglia (Lwigale, 2001) in neural crest ablated embryos and some loss of the ganglion (Lwigale, 2001) in placode ablated embryos. However, these analyses were performed at stages 34–35 or later, by which time a considerable amount of tissue regeneration may have occurred. To minimize such regulation, we removed broader tissue

regions encompassing the entire presumptive trigeminal placode or neural crest domains and analyzed the effects at times of cell ingression and ganglion formation. Our ablation experiments show that neural crest–placode interactions are prevalent and interdependent at early stages. Removal of neural crest results in dispersed placodal aggregates, and a lack of proper axonal trajectories to the brain and sensory organs. This suggests that neural crest cells make a scaffold on which placode cells organize. In the absence of this scaffold, placode cells appear to be able to aggregate, but do so with abnormal morphology. Additionally, neural crest cells may play a critical role in guiding placodal axons. Previous attempts of ablating the trigeminal placodes have so far been marked by incomplete placodal removal and regeneration and thus results were inconclusive (Hamburger, 1961; Stark et al., 1997). In our study, to minimize possible regeneration, we have conducted our ablations at later stages— at about 16 somite stage (late stage 11 to stage 12)— and also subsequently verified the extent of the placodal ablation by staining for placodal neurons. In many cases, we were successful in removing nearly all the placodal ganglion and in others most was removed except for a small placodal component. Both extents of ablation provided insightful information about the role of placodal cells on neural crest. From these data, we clearly demonstrate for the first time the dependence of neural crest on placodal cells in condensation into ganglion. We show that neural crest cells, by a mechanism that is currently unknown, appear to only assemble and coalesce in the same places as the placodal cells.

Similar coordination between neural crest and placode cells may be a general feature of all developing cranial ganglia of dual origin. For example, there is evidence that neural crest ablation disrupts central axon targeting of the epibranchial ganglia, suggesting that the neuroglial hindbrain crest cells may guide epibranchial placode cells into the mesenchyme and towards the central nervous system to establish their central projections (Begbie and Graham, 2001a). However, the underlying mechanisms were not clear.

2.5.2 Mechanism of Slit1–Robo2 on organizing trigeminal placodal cells and its indirect effect on neural crest

The complementary expression patterns of the Robo2 receptor in placode cells and its cognate ligand, Slit1, in the cranial neural crest raised the intriguing possibility that Slit–Robo signaling may be responsible for coordinating cell–cell interactions during trigeminal ganglion formation. To test this idea, we functionally perturbed Robo2 signaling *in vivo* and found that this results in delayed placodal ingression and migration to the trigeminal anlage. This in turn causes a dramatic disorganization of the forming placodal ganglion and secondarily, leads to abnormalities in the assembly of neural crest cells. The non-cell autonomous effect on neural crest cells is not surprising considering the high degree of interactions between neural crest and placodal cells during ganglion assembly that we found from our cell–cell interactions and ablation studies. Since Slit1 is a large, secreted molecule, it is unlikely that this is caused by reverse signaling in which Robo2 on placode cells activates Slit1 in neural crest cells. Rather it is likely to be mediated by other, as yet unknown, secondary factors. Effects of Robo2 inhibition on placode cells were similar to those of neural crest ablation that effectively removes the source of the ligand Slit1. This is supported by our RNAi data, showing that depleting either receptor or ligand causes malformation of the ganglion. The data support a mechanism whereby the Robo2 receptor on placode cells binds to the Slit1 ligand on neural crest cells to mediate proper ganglion assembly. This is the first demonstration of involvement of signaling molecules in trigeminal cell–cell interactions. In addition, Slit-independent functions of Robo2 may also occur, since Robo–Robo2 interactions have been implicated in other systems (Hivert et al., 2002; Parsons et al., 2003).

Our results reveal a novel role for Robo2 signaling as a mediator of cell–cell interactions during gangliogenesis. Ligand–receptor interactions between Slits and Robos

have been widely implicated in repulsive axon guidance in various aspects of nervous system development, such as commissural axon crossing in the central nervous system (Kidd et al., 1999) and formation of the lateral olfactory tract (Fouquet et al., 2007). The function of Slit as a repulsive cue at the midline is conserved across invertebrates (Kidd et al., 1999; Kidd et al., 1998) and vertebrates (Long et al., 2004). However, Slit1 does not seem to act as a repulsive signal between placode and neural crest, as we noted no evidence of avoidance or inhibitory behavior. In fact, both *in vivo* and *in vitro* analyses suggest that the neural crest and placode cells extensively intermix and contact one another throughout phases of migration and ganglion formation. Rather, the results suggest that these cell types intimately interact to reciprocally organize one another into the proper anatomical structure of the trigeminal ganglion. Consistent with our results, novel roles for Slit–Robo signaling have emerged more recently in the fly heart (Santiago-Martinez et al., 2006) and mammary duct (Strickland et al., 2006) where they function as cell adhesion and alignment cues. Our data suggest that Slit–Robo signaling acts as a positive regulator of placode ingression, cell positioning, and/or placode axon guidance during trigeminal gangliogenesis, consistent with a novel role in cell–cell interactions during morphogenesis. Intriguingly, Slit1 is down-regulated while Robo2 receptor expression persists, suggesting that interactions are time-limited. At later stages, it is possible that Robo2 might interact with itself or Slits in other tissues. Finally, we cannot rule out a possible function for Robo3 (Rig-1) and Robo4 in ganglion formation, since these are yet to be isolated in aves. However, based on their expression and function in other systems, this possibility seems unlikely since Robo4 is only expressed in endothelial cells with a function in angiogenesis (Park et al., 2003; Suchting et al., 2005), and its ability to bind to Slits is controversial (Suchting et al., 2005). Robo3 expression is known to be mainly restricted to the mammalian central nervous system where it acts as a negative regulator of Slit responsiveness (Sabatier et al., 2004).

2.5.3 Implications on the differences between OpV and MmV placodes

Although defects were observed in both trigeminal lobes, we observed more severe anomalies in the OpV than MmV lobes for both Robo2 perturbation (either using Robo2 Δ -GFP or Robo2 miRNA) and neural crest ablation. This may reflect inherent differences between the OpV and MmV placodes which arise from distinct regions to give rise to the respective OpV and MmV lobes of the trigeminal ganglion (Baker and Bronner-Fraser, 2001; D'Amico-Martel and Noden, 1983; Schlosser, 2005). This is consistent with the fact that these populations may be in part molecularly distinct in aves (Baker and Bronner-Fraser, 2001; Begbie et al., 2002), having mutually exclusive expression of Pax3 and neurogenin-2 (at least transiently) in the OpV and neurogenin-1 in the MmV placode. Furthermore, OpV and MmV placode cells are thought to be ancestrally separate. In amphibians, two separate ganglia form and later fuse (Northcutt and Brandle, 1995; Schlosser and Roth, 1997). Some gnathostomes, including basal ray-finned fishes and small-spotted dogfish sharks, have two distinct ganglia (O'Neill et al., 2007; Piotrowski and Northcutt, 1996; Schlosser, 2005), namely the profundal and trigeminal ganglia which are considered analogous to the OpV and MmV lobes in amniotes, respectively. Thus, although the Robo2 receptor is expressed by both OpV and MmV placode cells (albeit weaker expression in the MmV lobe), its role in cell-cell interactions may be more prominent in the OpV placode cells. Accordingly, a selective defect in arborization of the OpV branch was found in Slits and Robos mutant mice (Ma and Tessier-Lavigne, 2007), though gangliogenesis was not studied. Regardless of differences in severity of the defect, our data suggest that the Robo2 receptor plays a crucial role in mediating proper integration of the placode neurons in both lobes.

2.5.4 Possible downstream mechanism of Slit1–Robo2 in gangliogenesis

As a possible downstream mechanism, Slit activation of Robo has been shown to inhibit the cell adhesion molecule N-cadherin (Rhee et al., 2002) that has been implicated in formation of other peripheral ganglia (Kasemeier-Kulesa et al., 2006) and various morphogenetic events (Hatta and Takeichi, 1986). This raises the intriguing possibility that Slit–Robo interactions may regulate N-cadherin function in trigeminal precursors. In this scenario, the expression of Slit1 during early neural crest–placode interactions may be responsible for maintaining Robo2 expressing placode neurons in a less aggregated state, thus allowing intermixing of the two precursor cell types prior to their condensation. At later times when Slit1 is downregulated, N-cadherin may be upregulated and thus promote ganglionic condensation.

2.5.5 Conclusions

In summary, we demonstrate an essential function for the Robo2 receptor expressed by the trigeminal placodes in organizing both placodal neurons and Slit1-expressing neural crest cells into the proper anatomical structure of the trigeminal ganglion. This represents a previously unknown role for vertebrate Robo–Slit signaling in cell assembly and gangliogenesis. The results provide novel insights into cranial ganglion formation and, for the first time, a putative molecular signaling event underlying placode–neural crest interactions during aggregation of the largest of the cranial ganglia. Understanding the mechanisms that drive integration of the two embryonic structures that give rise to nearly all cranial ganglia sheds important light on the mechanisms mediating organization of the vertebrate sensory nervous system.

2.6 Acknowledgements

I thank Raman Das and Stuart Wilson for the design and construction of the RNAi vectors, Sarah Guthrie for the Robo2 Δ -GFP plasmid, Peter Lwigale for our work on the ablation and grafting experiments and many insightful discussions, and members of the MBF lab for technical support. This work was supported by NIH NRSA 5T32 GM07616 to C.E.S., NIH Minority Supplement grant DE016459-07S1 to P.Y.L., Biotechnology and Biological Sciences Research Council (U.K.) to R.D., and NIH grant DE16459 to M.B.F.

Figure 1.

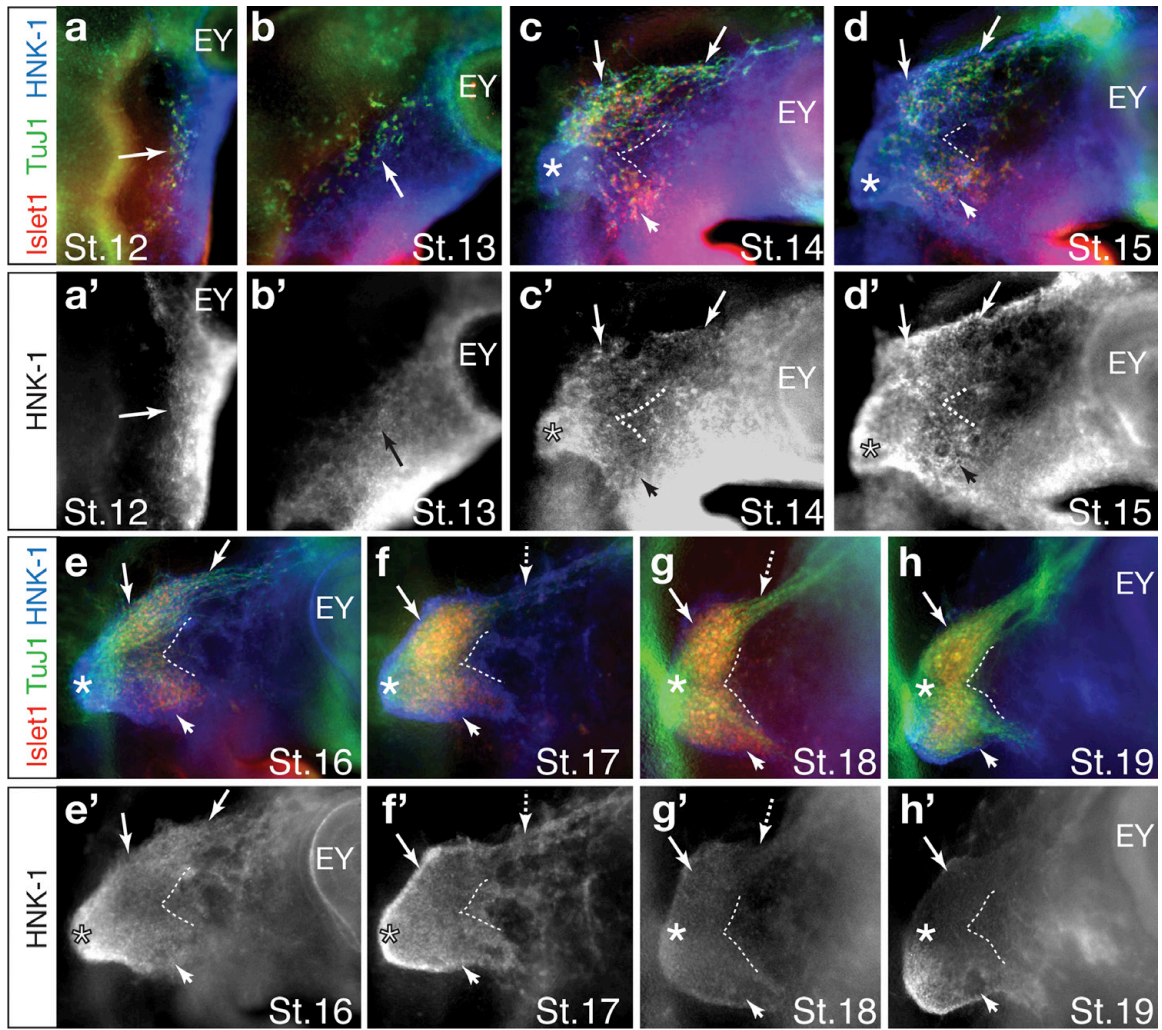


Figure 1. Chick embryos at successive stages between 12 and 19 show progressive development of the trigeminal ganglion. **(a–h)** During these stages, there is extensive overlap and intermingling of placodal and neural crest cell populations, as visualized using antibodies against Islet1 and TuJ1 for placodal cells and HNK-1 for neural crest cells (also shown in **a'–h'**). By stage 12, **(a)** several placodal cells can be detected diffusely distributed along the dorsal edge of the **(a')** neural crest stream (arrow) between the levels of the developing eye and anterior hindbrain. **(a–d)** From stages 12–15, the OpV placodal neurons (arrows) appear first and are already located more dorsally than the MmV placodal cells (arrowheads). Though diffuse, placodal cells already prefigure the morphology of the future bi-lobed ganglion. **(a'–h')** Assembly of trigeminal placodal cells takes place within the domain of the trigeminal neural crest stream throughout development; **(c)** by stage 14 the most proximal region (asterisk) already appears to be occupied by only neural crest cells. **(e)** By stage 16, the interlobic region (demarcated by the white dotted lines) that lies between the OpV and MmV lobes is mostly devoid of placodal neurons, and the trigeminal neural crest has begun to segregate from the periocular neural crest. This results in an increasingly more defined trigeminal morphology. **(f–g)** By stages 17–18, placodal and neural crest cells are well condensed into the ganglion and few placodal cell bodies are found along the OpV projection (dotted arrow). EY, eye; *, most proximal region to hindbrain.

Figure 2. Placodal neurons and neural crest cells intermingle intimately to form the ganglion in vivo. **(a–d)** Transverse sections of chick embryos showing neural crest and placodal cells at stages 12–15. Placodal neurons (Islet1+ and TuJ1+) begin to ingress from the ectoderm by stage 12 and continue to be generated in the ectoderm prior to undergoing an epithelial-to-mesenchymal transition to migrate into the same region as the HNK-1+ neural crest cells. Placodal cells make abundant cell contacts among themselves as well as with the neural crest cells. **(e–k)** Placodal and neural crest cells continue to exhibit intimate contacts throughout gangliogenesis, as visualized by GFP-labeled neural crest cells closely intermixing with Islet1+ placodal cells in the condensed ganglion at stage 17. **(e)** At stages of placodal condensation into the ganglion, the trigeminal neural crest cells also condense into the ganglion and have separated from the other neural crest populations which are surrounding the eye and migrating into the first branchial arch. **(f–k)** Neural crest cells labeled by GFP condense wherever the Islet1+ placodal cells are present, intermixing with placodal cells **(g, i–k)** in the ganglion lobe and **(h)** along the OpV projection. **(l)** A section through the trigeminal ganglion of an embryo that was electroporated with a GFP construct in the ectoderm; coexpression of neuronal marker Islet1 with GFP expression in the placode-derived cells at stage 17 affirms the placodal origin of the neurons. EY, eye.

Figure 3.

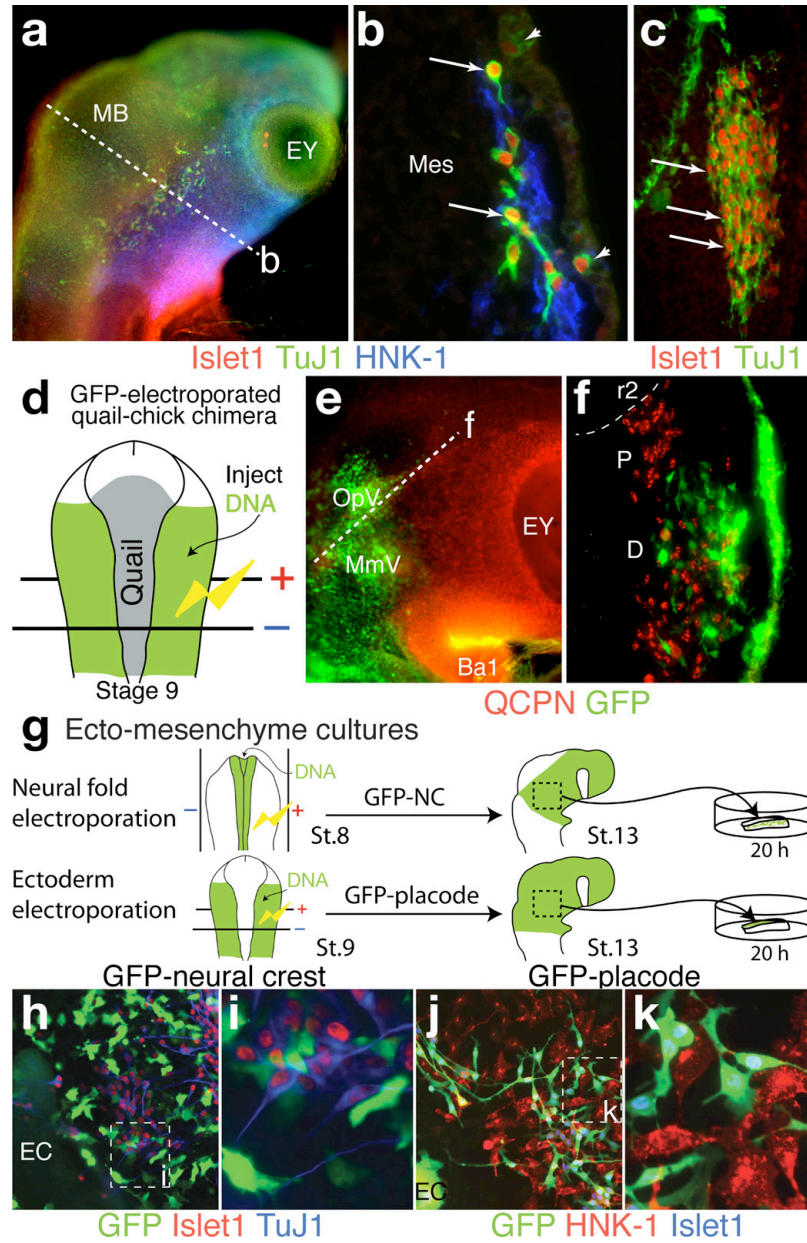


Figure 3. Placode and neural crest cells are in contact during trigeminal gangliogenesis. **(a)** Stage 13 chick and **(b)** cross section at the dotted line in **a** showing TuJ1+ and Islet1+ placodal cells (arrowheads) in the surface ectoderm and (arrows) in close contact with HNK-1+ neural crest cells. **(c)** Cross section through the OpV region of the condensed trigeminal ganglion at stage 17. **(d)** Schematic of chick embryo with ectoderm electroporated with a GFP construct and a quail neural fold graft. **(e)** Resulting chimera showing contribution of quail-derived neural crest cells (positive for the quail nuclear marker QCPN) and placodal cells (GFP+) in the stage 18 ganglion. **(f)** Transverse section through the OpV region at the dotted line in **e** showing distribution of QCPN+ neural crest cells and GFP+ placodal cells. **(g–k)** Using a tissue culture system to examine trigeminal placode–neural crest interactions. GFP labeling either the neural crest cells or the placodal cells show direct contacts between cytoplasmic protrusions of neural crest cells and the neuronal processes of placodal cells. MB, midbrain; EY, eye; Mes, mesenchyme; OpV, ophthalmic; MmV, maxillo-mandibular; Ba1, first branchial arch; r2, hindbrain rhombomere 2; P, proximal; D, distal; NC, neural crest; EC, ectoderm explant.

Figure 4.

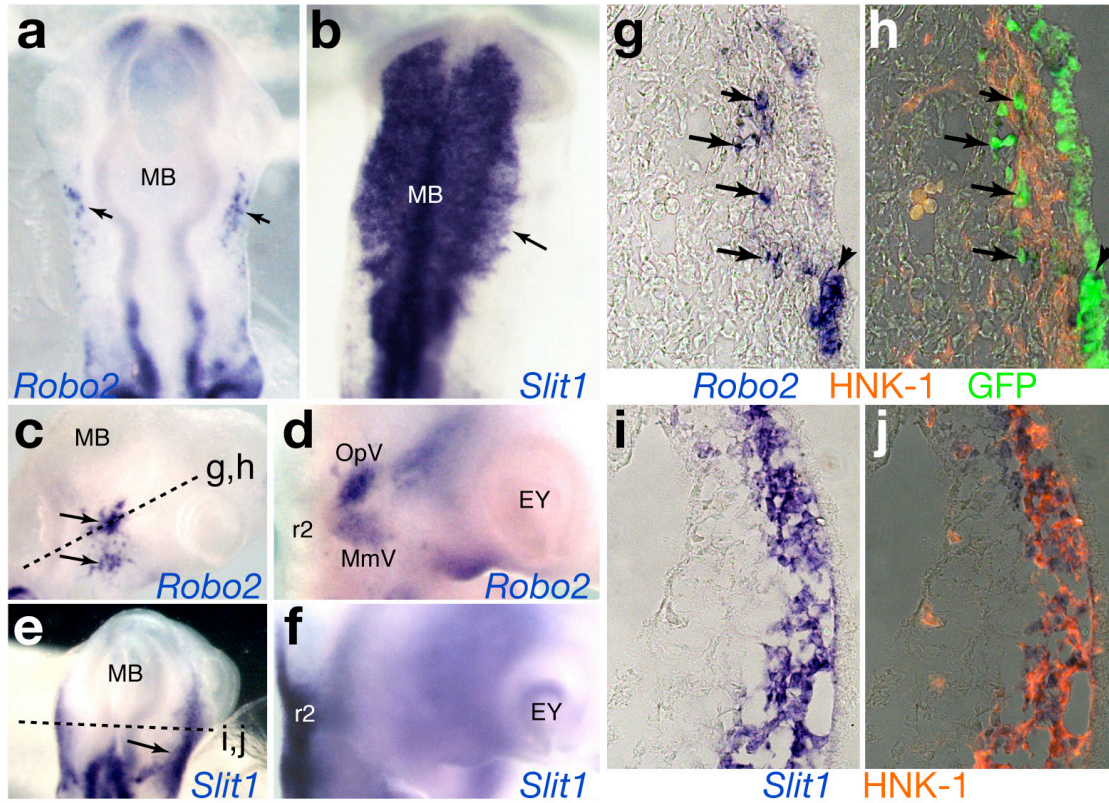


Figure 4. Expression of *Robo2* mRNA in placode and *Slit1* mRNA in neural crest cells during early development of the trigeminal ganglion. (a) Presumptive trigeminal placodal cells express *Robo2* (arrows) as they begin to ingress from the ectoderm. (b) Migratory cranial neural crest cells express *Slit1* (arrow) as early as stage 10. (c) *Robo2* is expressed in the OpV and MmV placodal cells at stage 14 (arrows) and (d) persists in the placodal component of the condensed ganglion at stage 18. (e) Trigeminal neural crest cells express *Slit1* at stage 13 (arrow) but (f) down-regulate *Slit1* in the ganglion by stage 18. (g) Transverse section through the OpV region at the dotted line in c shows *Robo2* expression both in the ectoderm (arrowhead) and ingressing placodal cells (arrows). (h) Overlay image of g, showing that *Robo2* expressing cells are GFP+, indicating their ectodermal origin, and intermingle with HNK-1+ neural crest cells. (i,j) Transverse section through the midbrain-hindbrain region of e shows (i) *Slit1* expression by (j) HNK-1+ migratory neural crest cells. MB, midbrain; EY, eye; r2, hindbrain rhombomere 2; OpV, ophthalmic; MmV, maxillo-mandibular.

Figure 5.

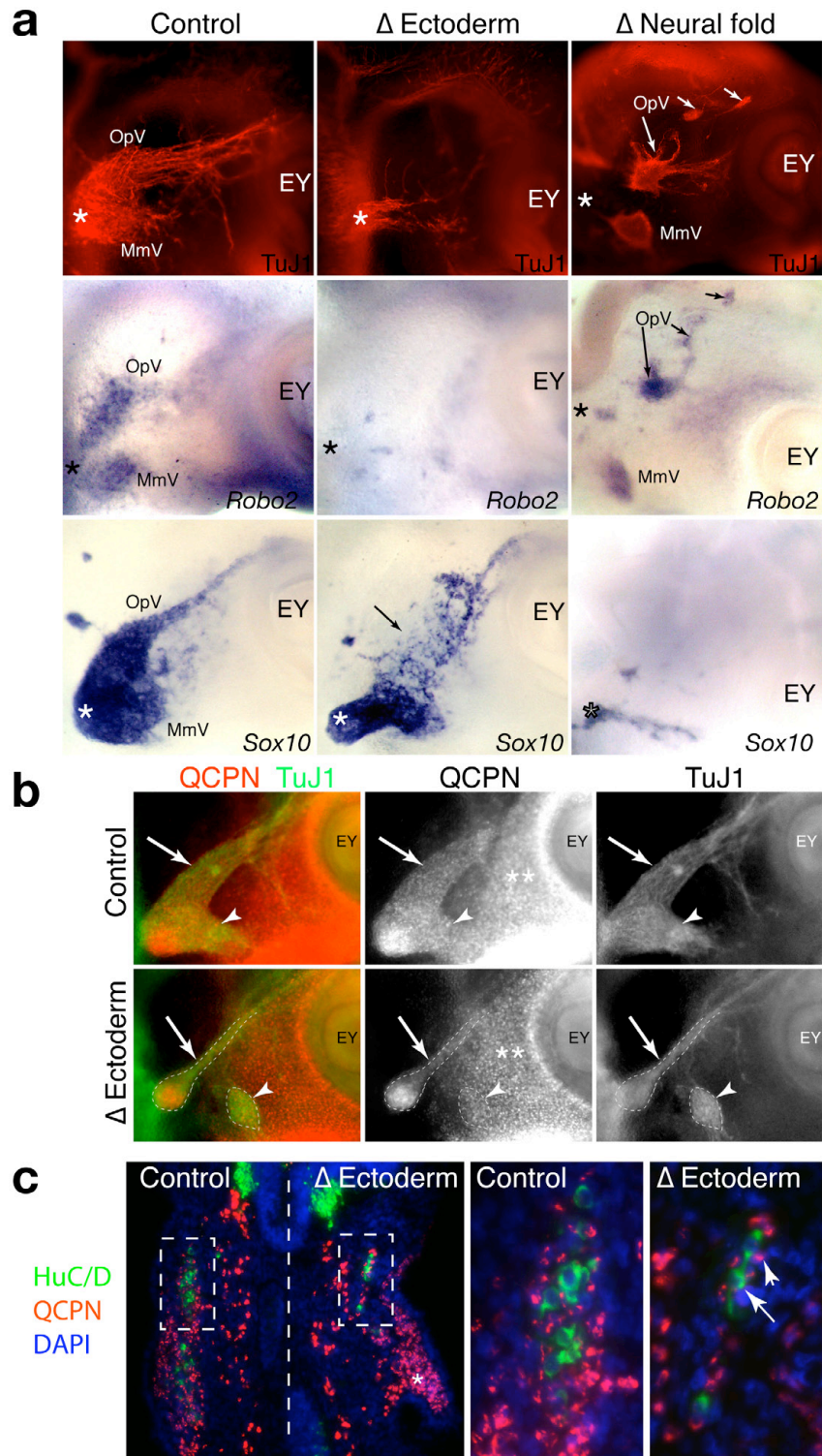


Figure 5. Proper formation of the trigeminal ganglion relies on reciprocal interactions between placodal and neural crest cells. **(a)** Unablated control sides show normal ganglion formation as revealed by placodal markers, TuJ1 protein and *Robo2* mRNA, and a neural crest marker, *Sox10* mRNA. Trigeminal ectoderm ablation (Δ) results in apparent removal of placode cells as shown by loss of TuJ1 and *Robo2*, and leads to aberrant neural crest condensation (*Sox10*, arrow), albeit aggregation in the most proximal region (*). Neural fold ablation leads to neural crest depletion as shown by loss of *Sox10* and results in unintegrated placodal aggregates (TuJ1+ or *Robo2*+, arrows), including disconnected OpV and MmV lobes. **(b)** Loss of neural crest condensation in placodal ectoderm ablated quail-chick chimeras. Unablated control side shows normal incorporation of QCPN+ neural crest and TuJ1+ placodes. In contrast, on ablated side of the same embryo, QCPN+ neural crest cells only condense in the region of placodal aggregation (dotted lines) formed by residual placodal cells, derived from regeneration or incomplete ablation; neural crest cells that do not condense in the ganglion appear dispersed in the periocular region (**). **(c)** Frontal plane section through an ectoderm ablated chimeric quail-chick embryo as that shown in **b** shows aggregation of quail derived neural crest cells (QCPN+) and placodal neurons (HuC/D+), and confirms that the neurons were not of neural crest origin. DAPI was used to stain all nuclei. On both the control and ablated sides, neural crest and placodal cells were found to intermix and form ganglion aggregates, albeit far fewer of them on the ablated side. On the ablated side, closely associating QCPN+ neural crest cells can be found only near the first branchial arch region (*) and not in the ganglion anlage. Each subpanel in **a** shows a different ablated embryo, except that the controls correspond to the same embryo as the adjacent ectoderm-ablated embryo. EY, eye; OpV or arrow, ophthalmic; MmV or arrowhead, maxillo-mandibular; *, in **a**, trigeminal region most proximal to the hindbrain.

Figure 6.

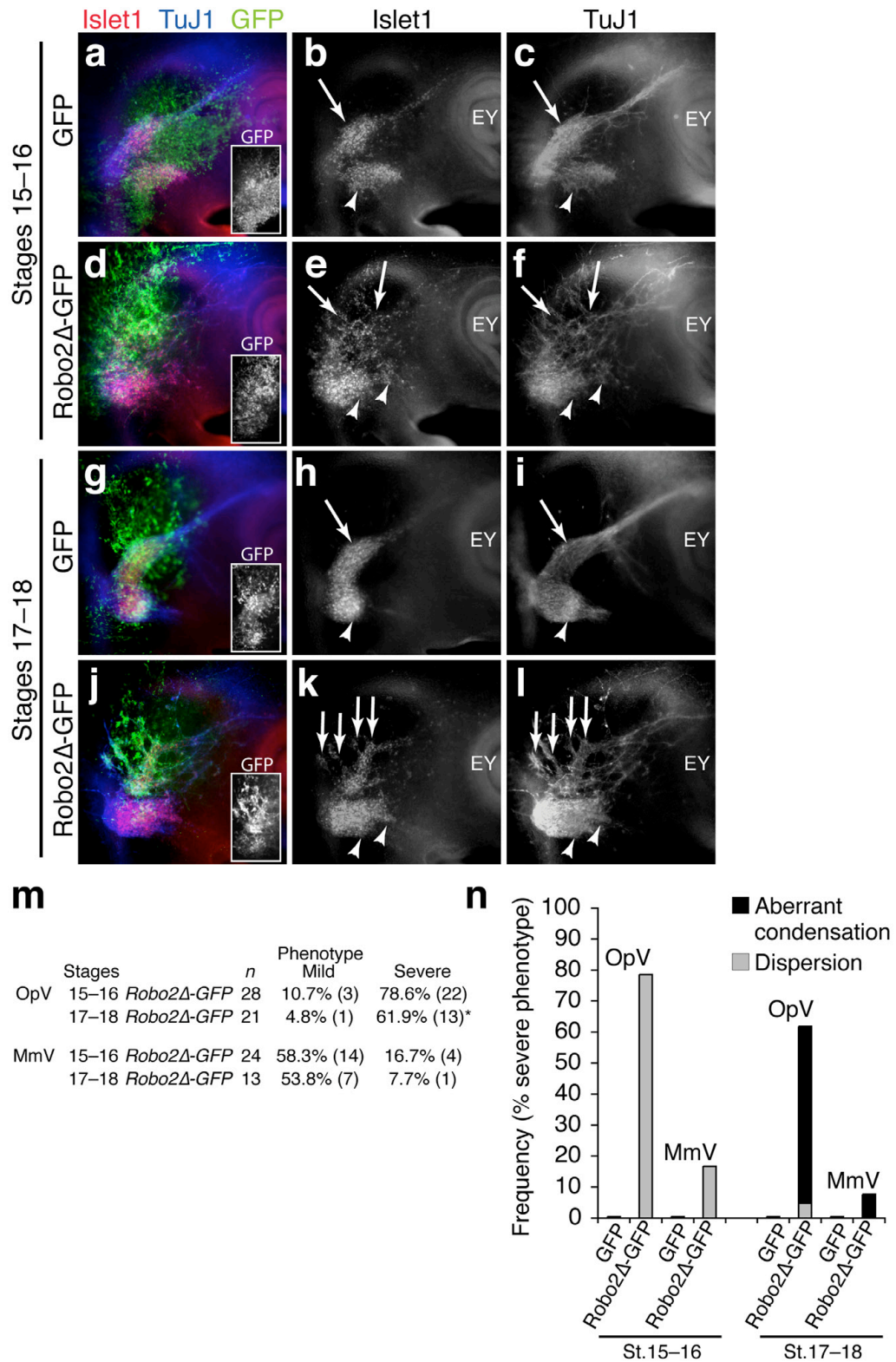


Figure 6. Inhibition of Robo2 signaling disrupts trigeminal ganglion formation. **(a–c)** Control GFP embryo and **(d–f)** Robo2Δ-GFP embryo at stages 15–16. **(g–i)** Control GFP embryo and **(j–l)** Robo2Δ-GFP embryo at stages 17–18. Placodal cell bodies (Islet1+) and neuronal processes (TuJ1+) are shown. GFP (green in color overlay panels; also shown in insets) reveals region of DNA transfection. **(m)** Effect of Robo2Δ-GFP is reported in two levels of severity: “mild” means intact but misshapen ganglia and “severe” means dispersion or aberrant condensation (branch-like or multiple aggregations) of the ganglia. Only one case (*) at stages 17–18 exhibited dispersion, and no aberrant condensation was observed at stages 15–16. Control GFP embryos showed no apparent phenotype at stages 15–16 in OpV ($n = 13$) and MmV ($n = 12$), and at stages 17–18 in OpV ($n = 22$) and MmV ($n = 21$). Numbers in parentheses represent the number of transfected ganglia showing the phenotype. **(n)** Histogram of data presented in **m** showing more severe effects in the OpV region. EY, eye; OpV or arrow, ophthalmic; MmV or arrowhead, maxillo-mandibular.

Figure 7.

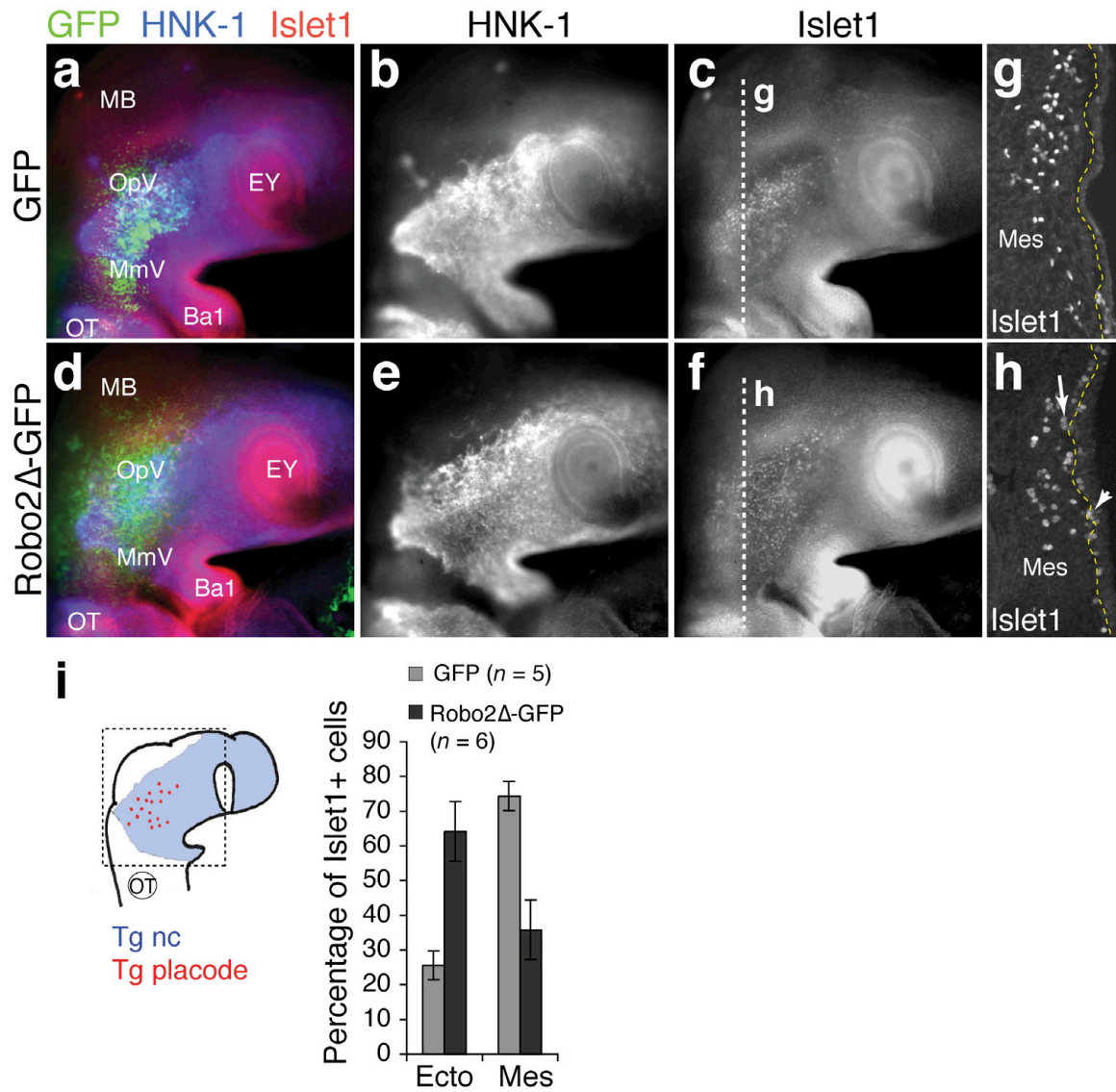


Figure 7. Inhibition of Robo2 signaling disrupts the ingression of trigeminal placodal cells. **(a–c)** Control GFP electroporated embryo analyzed at stage 14 showing **(a)** transfected GFP+ cells and **(b)** HNK-1+ neural crest cells and **(c)** Islet1+ placodal cells. **(d–f)** Robo2 Δ -GFP electroporated embryo analyzed at stage 14 showing that placodal cells (Islet1+, **f**) are more dispersed than in controls, but **(e)** HNK-1+ neural crest cell migration does not appear perturbed at this stage. **(g)** Frontal plane section through the control embryo at the dotted line in **c**, showing placodal cells (Islet1+). **(h)** Frontal section through the Robo2 Δ -GFP embryo in **f** reveals numerous placodal cells (Islet1+) remaining in the ectoderm (arrowhead) and adjacent to the basal margin (dotted line) of the ectoderm (arrow). **(i)** Left, schematic of a stage 14 chick embryo head showing the region of analysis (dotted box), encompassing the entire presumptive trigeminal area. Right, percentage of the total number of Islet1+ placodal cells associated with the ectoderm was significantly higher in Robo2 Δ -GFP than in control GFP embryos. Bars indicate s.d.; $P < 0.0001$, two-tailed Student's t-test. EY, eye; OpV, ophthalmic; MmV, maxillo-mandibular, Ba1, first branchial arch; Mes, mesenchyme; Ecto, ectoderm; Tg, trigeminal; nc, neural crest.

Figure 8.

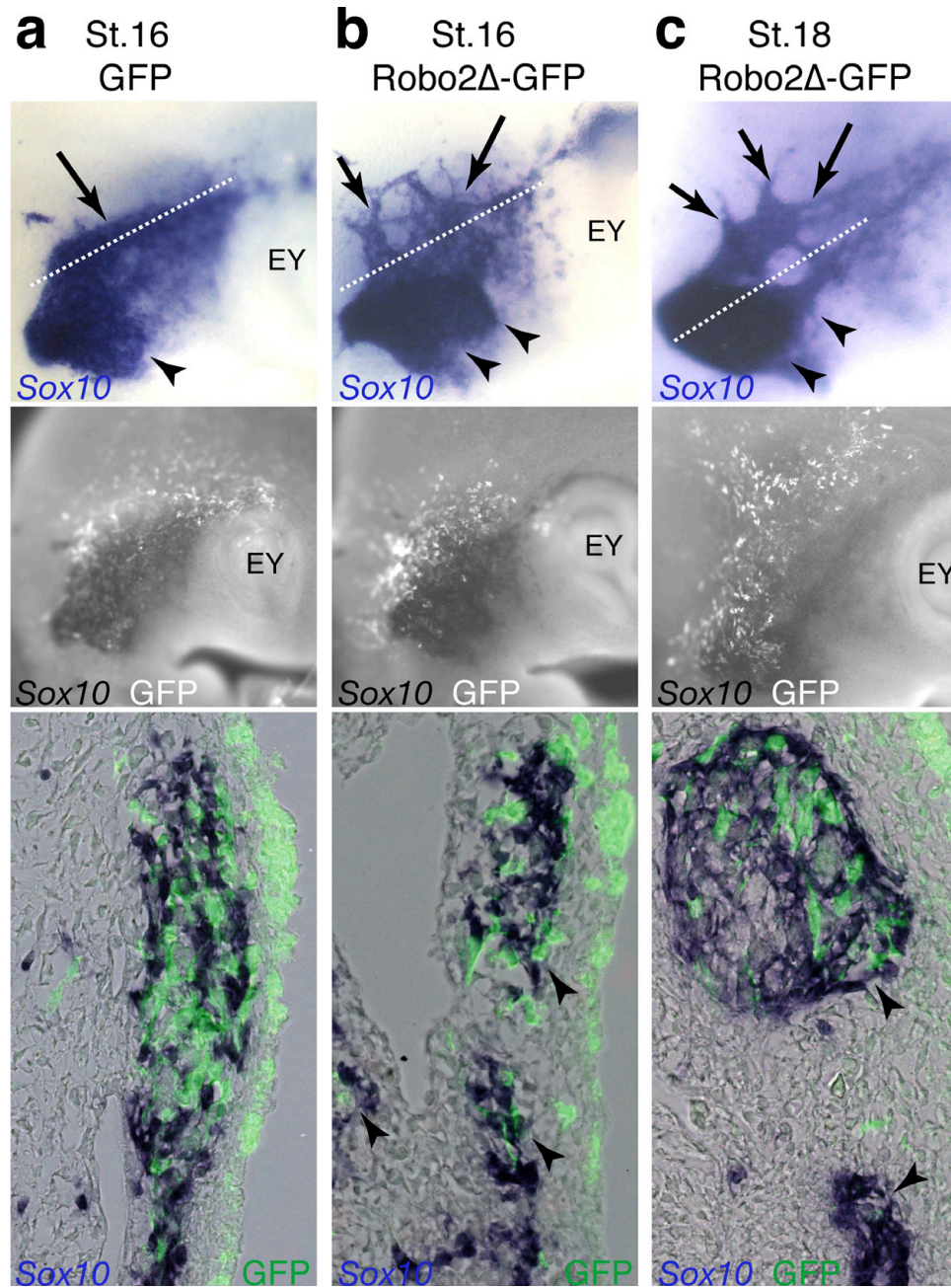


Figure 8. Inhibition of Robo2 signaling disrupts neural crest aggregation into the trigeminal ganglion. In situ hybridization with *Sox10* to label neural crest cells after electroporating ectoderm with the control GFP or Robo2 Δ -GFP construct. **(a)** Stage 16 control embryo showing *Sox10* expression in the trigeminal region overlapping with GFP expression (middle panel). Cross section (bottom panel) through the OpV lobe at dotted line in the top panel shows that *Sox10* expressing neural crest cells assemble together with GFP expressing placodal cells in one cluster. **(b)** Stage 16 embryo electroporated with Robo2 Δ -GFP showing dispersion of *Sox10* expressing neural crest cells in the OpV lobe (arrows) and formation of a misshapen MmV lobe (arrowheads, top panel) which correlates with the dispersion of Robo2 Δ -GFP expressing placodal cells. Cross section through the OpV lobe shows that *Sox10* expressing neural crest cells assemble wherever the Robo2 Δ -GFP expressing placodal cells are clustered (arrowheads, bottom panel). **(c)** The effect of inhibiting Robo2 signaling in placodal cells on neural crest persists even later at stage 18 after the ganglion is well condensed. Cross section through the dispersed region of the ganglion shows that *Sox10* expressing neural crest cells form branch-like aggregates corresponding to where the Robo2 Δ -GFP expressing placodal cells are clustered (arrowheads, bottom panel). EY, eye.

Figure 9.

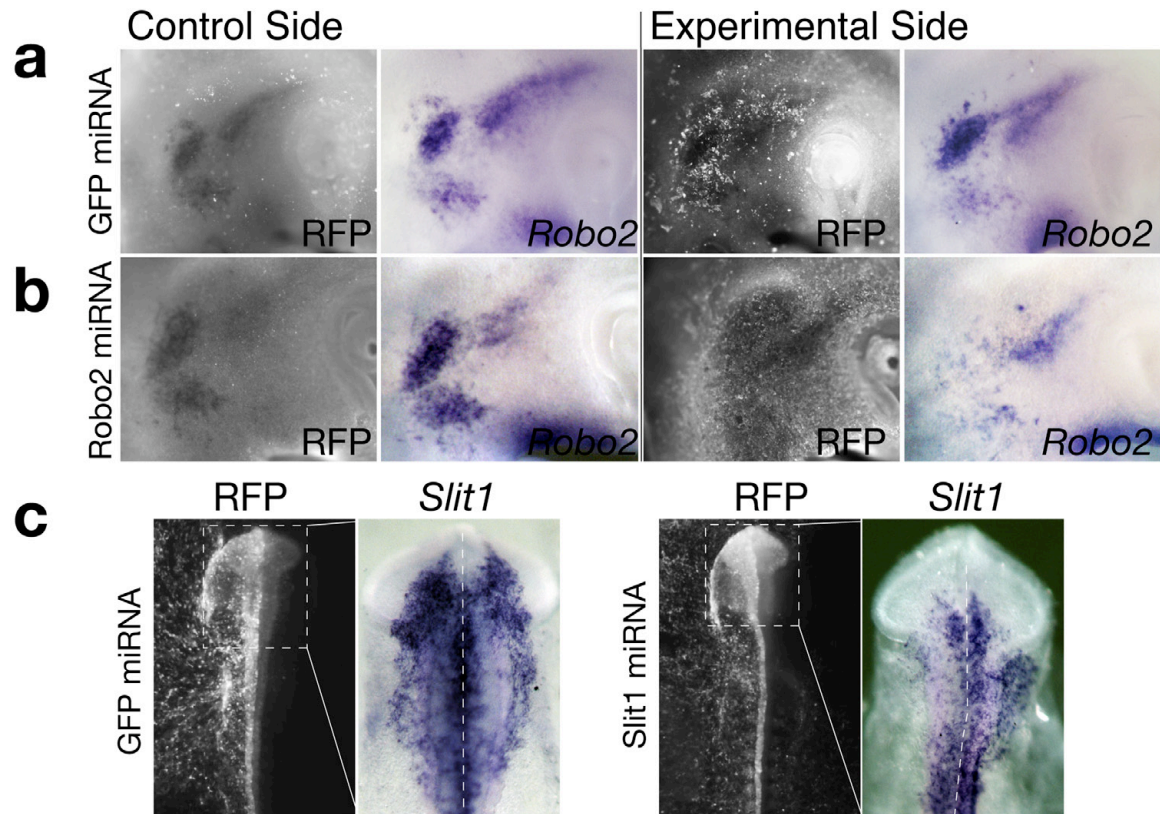


Figure 9. *Robo2* and *Slit1* RNAi constructs deplete *Robo2* and *Slit1* transcripts. (a, b) Embryos were electroporated with the RNAi vectors in the trigeminal ectoderm at stages 8–10 and then assessed for *Robo2* depletion by in situ hybridization in the trigeminal ganglion at stages 15–18. Control (which lacks RNAi) and experimental sides (with RNAi and RFP marker expression) were compared in each embryo. In contrast to the control GFP miRNA embryo in a, a marked depletion of *Robo2* is detected in the *Robo2* miRNA embryo in b. (c) Embryos were electroporated with the RNAi vectors on the left side at stages 4–6 and then assessed for *Slit1* knockdown in the premigratory and migratory neural crest cells at stages 8–10. Control GFP miRNA electroporated embryo displays normal *Slit1* expression whereas the *Slit1* miRNA electroporated embryo shows reduction of *Slit1* expression on the side with the RNAi vector expression (RFP+).

Figure 10.

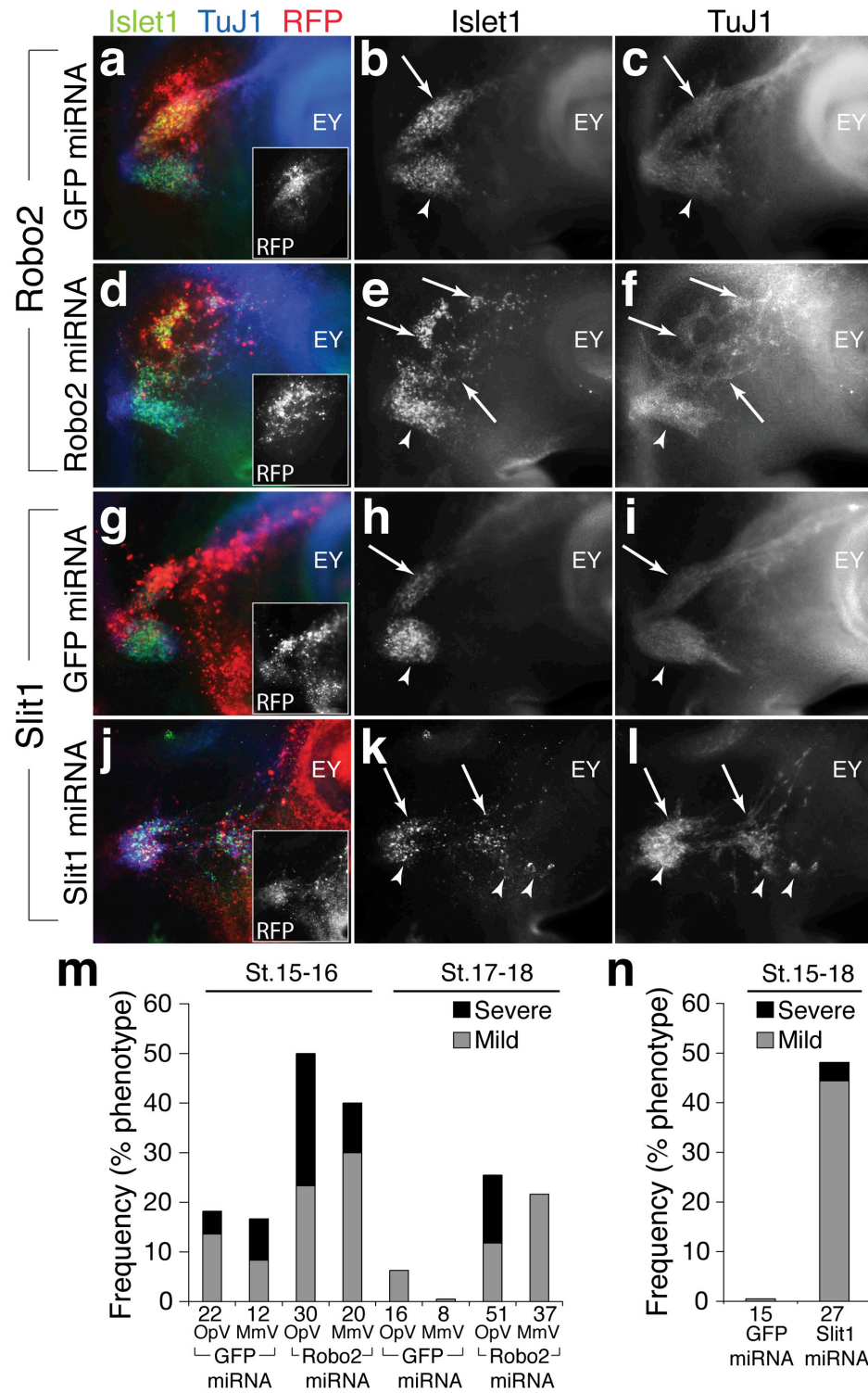


Figure 10. RNAi-mediated knockdown of Robo2 or its ligand Slit1 causes abnormal trigeminal ganglion assembly. (a–c) Control embryo electroporated with GFP miRNA in the trigeminal ectoderm at stage 16. (d–f) Robo2 miRNA embryo at stage 16. Both placodal cell bodies (Islet1+) and neuronal processes (TuJ1+) form abnormal clusters and branch-like aggregates in the OpV and interlobic regions (arrows); the MmV which lacks RNAi is relatively normal. (g–i) Control embryo electroporated with GFP miRNA in the neural crest at stage 17. (j–l) Slit1 miRNA embryo at stage 17. Placodal neurons are disorganized and form aberrant aggregates, and are often found dispersed and/or occupying the interlobic region. Histograms show that (m) Robo2 RNAi and (n) Slit1 RNAi embryos showed markedly higher percentages of trigeminal ganglion defects than the controls. Phenotypes considered as severe include aberrant condensation into dispersed or branch-like clumps or widespread cell dispersions, and as mild were regional cell dispersion or misshapen lobe, including displacement or misalignment of OpV and MmV lobes. Numbers below the bars are numbers of transfected ganglia analyzed. EY, eye; OpV or arrow, ophthalmic; MmV or arrowhead, maxillo-mandibular.